CO2-induced destabilization of pyrite-structured FeO2Hx in the lower mantle

Eglantine Boulard, François Guyot, Nicolas Menguy, Alexandre Corgne, Anne-Line Auzende, Jean-Philippe Perrillat, Guillaume Fiquet

HAL Id: hal-02110010

https://hal.sorbonne-universite.fr/hal-02110010v1

Submitted on 15 Dec 2021

GEOSCIENCES

CO$_2$-induced destabilization of pyrite-structured FeO$_2$Hx in the lower mantle

Eglantine Boulard[1,2,*], François Guyot[2], Nicolas Menguy[2], Alexandre Corgne[3], Anne-Line Auzende[4], Jean-Philippe Perrillat[5] and Guillaume Fiquet[2]

ABSTRACT

Volatiles, such as carbon and water, modulate the Earth's mantle rheology, partial melting and redox state, thereby playing a crucial role in the Earth's internal dynamics. We experimentally show the transformation of goethite FeOOH in the presence of CO$_2$ into a tetrahedral carbonate phase, Fe$_4$C$_3$O$_{12}$, at conditions above 107 GPa—2300 K. At temperatures below 2300 K, no interactions are evidenced between goethite and CO$_2$, and instead a pyrite-structured FeO$_2$H$_x$ is formed as recently reported by Hu *et al.* (2016; 2017) and Nishi *et al.* (2017). The interpretation is that, above a critical temperature, FeO$_2$H$_x$ reacts with CO$_2$ and H$_2$, yielding Fe$_4$C$_3$O$_{12}$ and H$_2$O. Our findings provide strong support for the stability of carbon-oxygen-bearing phases at lower-mantle conditions. In both subducting slabs and lower-mantle lithologies, the tetrahedral carbonate Fe$_4$C$_3$O$_{12}$ would replace the pyrite-structured FeO$_2$H$_x$ through carbonation of these phases. This reaction provides a new mechanism for hydrogen release as H$_2$O within the deep lower mantle. Our study shows that the deep carbon and hydrogen cycles may be more complex than previously thought, as they strongly depend on the control exerted by local mineralogical and chemical environments on the CO$_2$ and H$_2$ thermodynamic activities.

Keywords: deep carbon cycle, FeOOH, high pressure

[1]Synchrotron SOLEIL, 91192 St Aubin, France; [2]Sorbonne Université, Muséum National d'Histoire Naturelle, UMR CNRS 7590, IRD.—IMPMC, 4 Place Jussieu, 75005 Paris, France; [3]Instituto de Ciencias de la Tierra, Universidad Austral de Chile, 5090000 Valdivia, Chile; [4]ISTerre, Université Grenoble Alpes, CNRS, F-38041 Grenoble, France and [5]Laboratoire de Géologie de Lyon, UMR CNRS 5276, Université Claude Bernard Lyon 1—ENS de Lyon, 69622 Villeurbanne, France

*Corresponding author: E-mail: eglantine.boulard@upmc.fr

INTRODUCTION

Water (H$_2$O) and carbon dioxide (CO$_2$) both play an important role in the history of the Earth, as they strongly influence the chemical and physical properties of minerals, melts and fluids. Distribution and circulation of H$_2$O and CO$_2$ between the Earth's surface and the mantle have dominated the evolution of the crust, the oceans and the atmosphere, controlling several aspects of the Earth's habitability. It is therefore crucial to determine the stability and circulation of hydrous and CO$_2$-bearing minerals in the Earth's interior. Sedimentary material together with altered mafic and ultramafic rocks that constitute the subducted slabs represents the main source for recycling of H$_2$O and CO$_2$ as well as other volatiles at great depth, possibly down to the core—mantle boundary. The transport of H$_2$O and CO$_2$ via subducting slabs down to the transition zone and to the lower mantle has been the subject of many studies but is still under debate [1,2]. As for the carbon cycle, carbonates preserved during subduction are estimated to account for a flux of 3.6×10^{12} mol/year of carbon being returned into the deep mantle [3–5]. This quantity accounts for 10–30 wt % of the carbon reservoir in the deep mantle [6]. Regarding the water cycle, Van Keken *et al.* [2] suggested that 4–6×10^{13} mol/year of H$_2$O are recycled into the mantle through slab subduction. Dehydration of the slab accounts for the loss of two-thirds of this amount of H$_2$O, while one-third of the H$_2$O remains bounded to the slab (i.e. $\approx 1.5 \times 10^{13}$ mol/year) reaching depths exceeding 240 km. Although this amount of H$_2$O entering the deep mantle may not appear very large, it provides a mechanism for having significant amounts of water in the deep mantle. In addition, part of the CO$_2$ and H$_2$O present in the deep mantle may also originate from primitive mantle reservoirs [7], leading potentially to fairly large amounts of these volatiles in the deep mantle.

Because of its very low solubility in deep Earth's minerals [8,9], carbon is expected to be present

as accessory phases in the mantle, either as oxidized phases such as carbonates or CO_2 and carbonated fluids or melts, or as reduced phases such as diamonds or Fe-C alloys [10]. It is commonly considered that the lower mantle is too reducing to host carbonates [11,12]. However, the relatively high oxygen fugacities prevailing in subducting slabs might contribute to preserve oxidized carbon-bearing phases in the deep mantle [13,14]. Moreover, it has recently been demonstrated that carbonates at lower-mantle conditions adopt oxidized iron-bearing structures based on CO_4 tetrahedra that are associated with reduced carbon phases [13,15–17]. Little is known about the stability of these new tetrahedral carbon-bearing phases but their systematic association with reduced carbon suggests the idea that the mineralogies of the lower mantle and D″ region may be more complex than previously thought. Interestingly, carbonate-bearing inclusions have also been reported in diamonds formed in the lower mantle. This suggests again the presence of carbonates in the deep Earth and a possible coexistence of reduced and oxidized carbon species [15,18,19]. Decarbonation reactions of carbonates involving silicates (SiO_2 and $MgSiO_3$) were also reported to take place as shallow as ∼600 km in depth (20 GPa) [20,21]. Such reactions could produce CO_2 in the lower mantle. Given the current uncertainties on the phase diagram of CO_2 at high pressures, CO_2 may be expressed as a solid CO_2-V phase [21] or rather dissociate as C + O_2 [22]. Carbonated fluids yet unknown at such conditions might also contribute to CO_2 transfer at large depth in the mantle. In any case, large thermodynamic activities of CO_2 are plausible in the lower mantle.

A significant amount of water can be dissolved in nominally anhydrous minerals such as olivine, garnet and stishovite [23], as well as in high-pressure silicates such as wadsleyite and ringwoodite [24,25]. In addition, diverse dense hydrous silicates are stable in mafic and ultramafic assemblages at upper- and lower-mantle conditions, such as phase A, phase D, phase H and superhydrous phase B [26–30]. Finally, δ-AlOOH, a high-pressure form of diaspore (α-AlOOH) with an orthorhombic symmetry very close to that of the $CaCl_2$-type polymorph of SiO_2, is stable throughout the mantle and may be present in suitably aluminous and hydrated lithologies [31,32]. The high-pressure polymorph ε-FeOOH that shares the same structure with δ-AlOOH [33] might also store water in the mantle. Iron oxyhydroxides, including FeOOH and its polymorphs, are common at the surface of the Earth, where they are abundant in soils and sediments. The incorporation of hydrogen atoms in newly discovered iron oxyhydroxides with a pyrite structure [34–36] may thus contribute to the

transfer of H to the deep Earth. In their recent work, Hu *et al.* [34] suggested that a phase of FeO_2H_x composition might indeed deliver H_2 instead of water when heated above a threshold temperature—a particularity due to valence changes of oxygen in this compound (from $2O^{2-}$ to O_2^{2-}) [37].

After H_2O, CO_2 is the second most important volatile compound in the deep Earth. To get a more complete understanding of the H and C cycles in the deep Earth, it is necessary to know how deep subducted materials can transport both C and H and identify the distinct species involved. In the present study, we shed light on this crucial issue by constraining experimentally the interactions of CO_2 with potential carriers of H_2O or H_2 at great depths. We performed high-pressure and high-temperature diamond-anvil cell (DAC) experiments to investigate the effects of a CO_2-rich medium on the transformations of FeOOH at pressures and temperatures of the lower mantle.

RESULTS

A natural sample of crystalline α-FeOOH (Supplementary Fig. 1) was loaded in CO_2 and first pressurized up to 107 GPa in a DAC at ambient temperature. *In situ* X-Ray diffraction (XRD) patterns showed a significant broadening of α-FeOOH main diffraction reflections characteristic of incipient amorphization. After laser heating at 2000 K for a few minutes, several changes in the diffraction pattern were observed: the α-FeOOH phase disappeared and two distinct phases were identified (Fig. 1). The most intense diffraction peaks correspond to a cubic structure with extinctions of the two reflections 001 and 011 in agreement with a Pa-3 space group. Recently, Hu *et al.* [34] reported the transformation of FeOOH into a new Pa-3 cubic structure FeO_2H_x at similar pressure and temperature conditions. This phase is directly related to the newly discovered pyrite-structured FeO_2 peroxide but is characterized by a larger unit cell volume [34,37]. FeO_2H_x can be interpreted as a solid solution between pyrite-structure FeO_2 and FeOOH. In addition, a pyrite-structured FeOOH oxyhydroxide (i.e. FeO_2H_x with x = 1) was recently observed experimentally by Nishi *et al.* [35]. It presents a structure close to the pyrite-type structure of AlOOH predicted above 170 GPa by Tsuchiya and Tsuchiya [38]. Here, we measured a unit cell parameter of a = 4.367 Å at 107 GPa, which is significantly larger than that reported for FeO_2 (a = 4.363 Å at 76 GPa) by Hu *et al.* [37], but smaller than that reported for FeOOH (a = 4.386 Å at 109 GPa) in Nishi *et al.* [35] (Fig. 2). It is thus probable that FeOOH in our
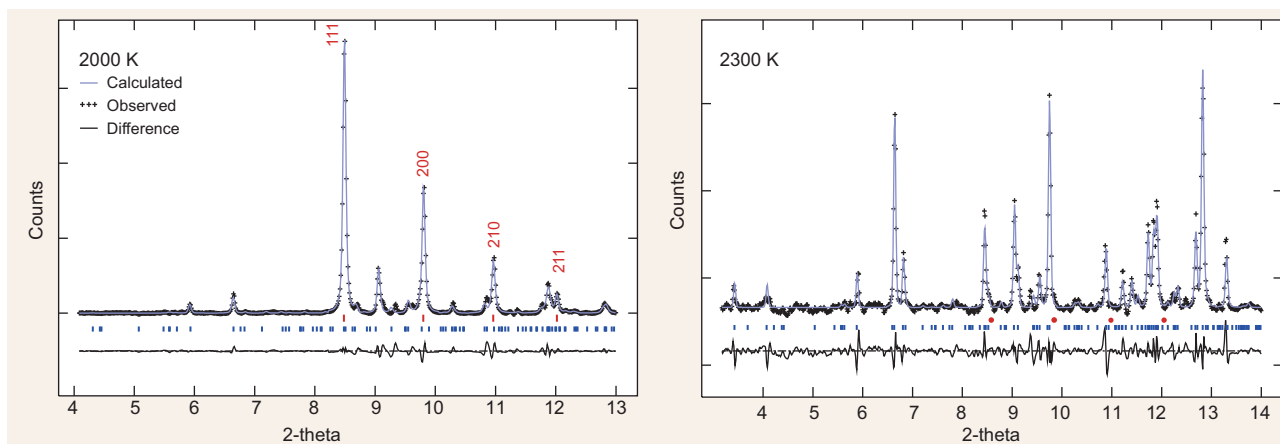
Figure 1. XRD patterns collected at 2000 K and at 2300 K and LeBail unit cell refinement of the two phases FeO_2H_x (red markers, space group Pa-3, a = 4.365(1)) and $Fe_4C_3O_{12}$ (blue markers, space group P2, a = 9.697(2), b = 6.296(2), c = 5.726(1), beta = 92.94(2)). Red circles materialize the expected peak position of the cubic phase according the XRD collected at lower temperature.

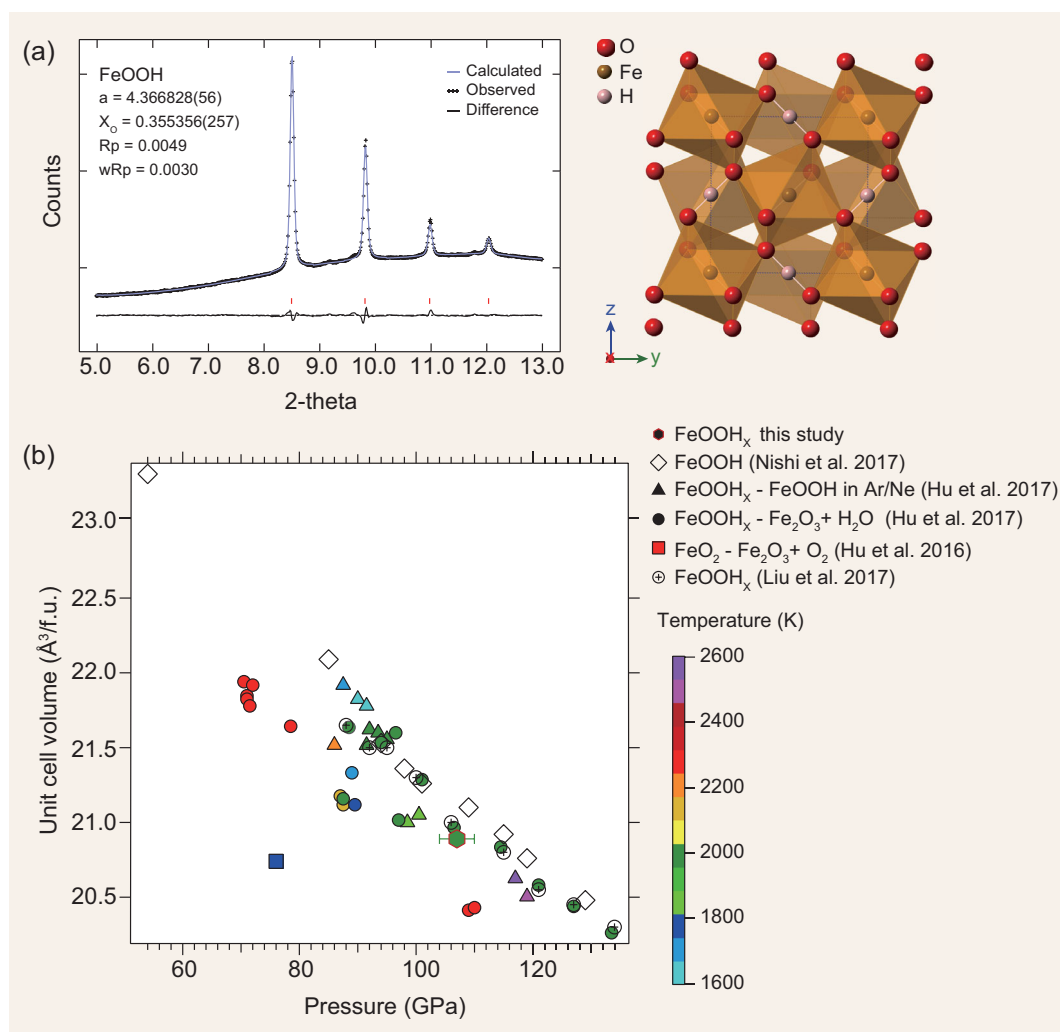**Figure 2.** (a) Rietveld refinement of the XRD pattern collected at 107 GPa and 300 K after laser heating with a FeO_2H pyrite-structured (right hand). (b) Unit cell volume of the pyrite-type structure measured experimentally as a function of pressure and temperature for FeO_2 [37], FeO_2Hx ([31], from both $Fe_2O_3+H_2O$ and FeOOH in Ar experiments and this study) and FeOOH [35]. All the data reported here were collected after quenching the temperature.
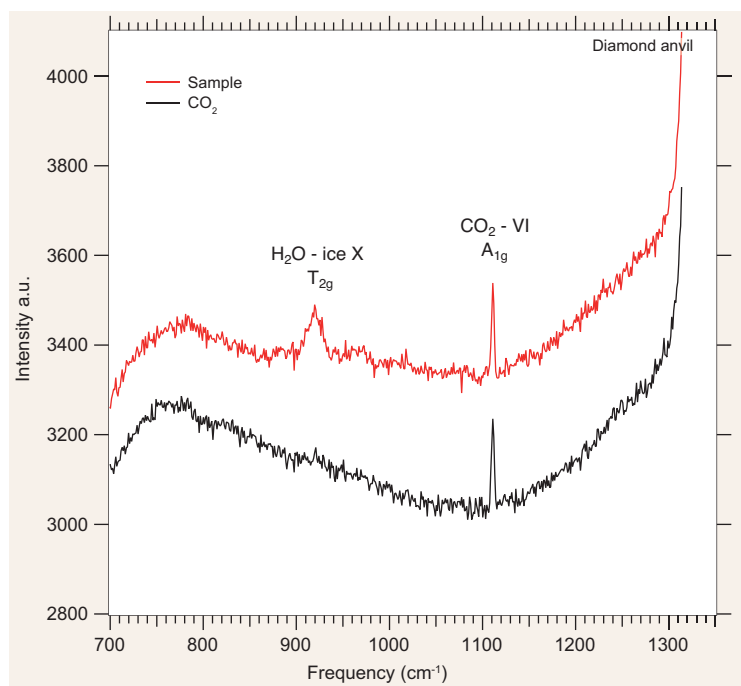
Figure 3. Raman spectra collected after laser heating in the CO_2 area (in black) and sample area (in red).

study underwent partial dehydrogenation. A similar unit cell volume based on a FeO_2H_x formula was reported at the same P-T conditions by Hu *et al.* [34], for which, using their calibration, they deduced x = 0.66. Because this calibration is not only built using experimental data, but also incorporates theoretical results, which are known to either overestimate or underestimate unit cell volume, uncertainty on the exact amount of hydrogen 'x' present in FeO_2H_x may be high. To account for this, we simply refer to this phase as FeO_2H_x.

In the XRD pattern, the less intense diffraction peaks can be assigned to an already discovered carbon-rich phase stable at these P-T conditions: $Fe_4C_3O_{12}$ [15] (Fig. 1). Among the five structures proposed in literature [15,17,39,40], we found that only the monoclinic structure reported in [15] allowed us to assign all of the observed diffraction peaks. Although *ex situ* analyses of the hydrogen content of this phase would be necessary, the fact that we measured unit cell parameters in very good agreement with that reported in [15] for a hydrogen-free composition leads us to propose an $Fe_4C_3O_{12}$ stoichiometry. Upon heating at higher temperature, diffraction peaks of $Fe_4C_3O_{12}$ increase in intensity at the expense of the FeO_2H_x cubic phase, which fully disappears above 2300 K (Fig. 1). Neither iron oxides (e.g. Fe_3O_4, Fe_2O_3, Fe_4O_5, $Fe_{13}O_{19}$) nor diamond were observed in these experiments. We

note that Fe in $Fe_4C_3O_{12}$ is ferric iron Fe(III) as in FeOOH. After laser heating, we collected a profile of diffraction patterns across the heated spot (Supplementary Fig. 2). The FeO_2H_x cubic phase was observed at the edge of the 2300-K heated spot only. Although it is theoretically possible that the reaction is kinetically restricted at lower temperatures, the fact that a change occurred abruptly at around 2300 K (FeO_2H_x disappears within a few seconds) more probably pinpoints to a thermodynamic boundary. The pyrite-structured FeO_2H_x would be stable only at relatively low temperatures in the Fe-O-C-H system provided CO_2 thermodynamic activities are high enough. Further studies should verify this point.

Raman spectra were also collected at ambient temperature and high pressure in the 300–1300 cm^{-1} range. As presented in Fig. 3, when collected in areas where the CO_2 loading gas was pure, the spectra reveal only one low intensity mode at ~1123 cm^{-1}, which corresponds to the most intense mode A_{1g} of CO_2-VI [41]. In the solid sample area, an additional mode was detected at ~930 cm^{-1} assigned to the T_{2g} mode from the high-pressure phase of H_2O ice-X [42,43]. No Raman active modes associated with $Fe_4C_3O_{12}$ could be observed, which may be due to high fluorescence background of the diamond from the DAC.

Transmission electron microscopy (TEM) analyses of a thin section extracted from the recovered sample are reported in Fig. 4. Semi-quantitative chemical analyses (XEDS) showed a homogenous composition with carbon, iron and oxygen with Fe-O atomic proportions consistently with $Fe_4C_3O_{12}$ (Fig. 4A). The sample was unstable under electron beam, and selective area electron diffraction (SAED) revealed the presence of two patterns (Fig. 4B): γ-Fe_2O_3 maghemite coexisting with a phase characterized by a 6-fold symmetry diffraction pattern that could not be indexed. It is probable that, under the electron beam, $Fe_4C_3O_{12}$ underwent carbon loss to form γ-Fe_2O_3 together with a second phase still containing carbon. Note that the observed texture, often observed in cases of irradiation damages, is in agreement with amorphization and devolatilization of the sample under the electron beam (Fig. 4C).

DISCUSSION

This study demonstrates that, at pressures of about 110 GPa and upon laser heating, a chemical reaction occurs between FeO_2H_x and CO_2 yielding a tetrahedral carbonate $Fe_4C_3O_{12}$. The transformation from the initial goethite FeOOH with increasing
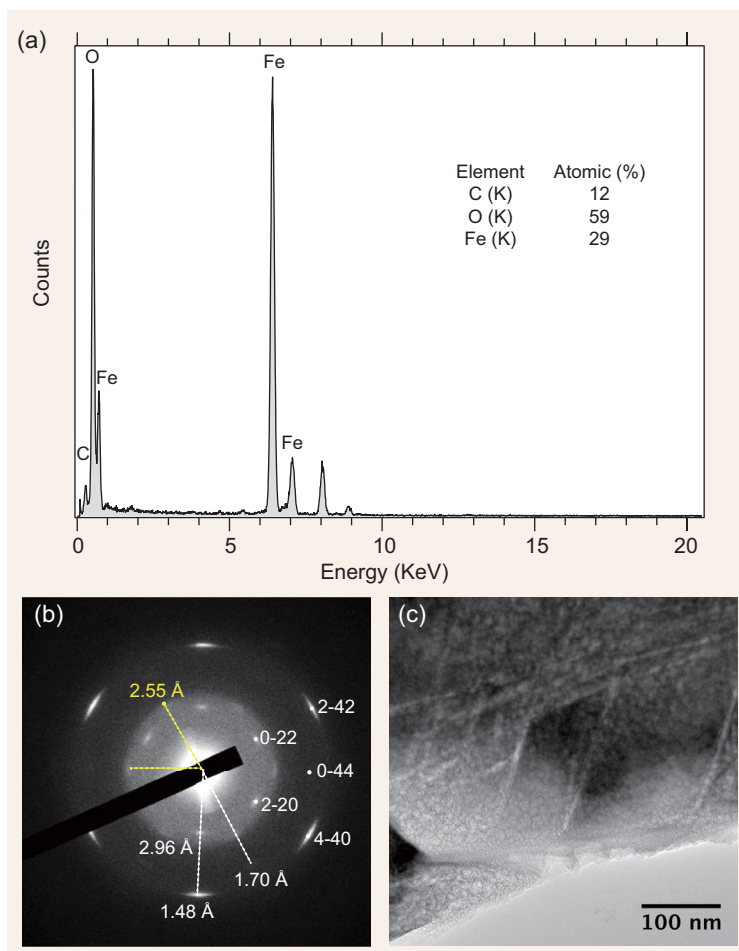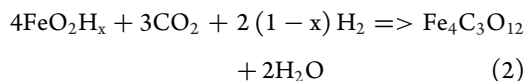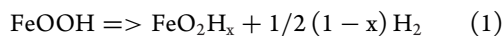
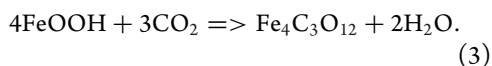**Figure 4.** (a) Semi-quantitative chemical analyses (EDX); (b) electron diffraction of Fe_2O_3 maghemite (white markers) together with an unknown phase (yellow markers); and (c) TEM picture of the sample after analyses.
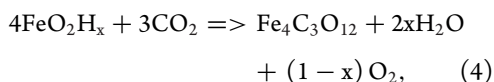
temperature can be schematized as:

$$FeOOH => FeO_2H_x + 1/2 \, (1-x) \, H_2 \qquad (1)$$

$$4FeO_2H_x + 3CO_2 + 2 \, (1-x) \, H_2 => Fe_4C_3O_{12} + 2H_2O \qquad (2)$$

which can be summed up as:

$$4FeOOH + 3CO_2 => Fe_4C_3O_{12} + 2H_2O. \qquad (3)$$

If the local thermodynamic activity of H_2 is too low for reaction (2) to proceed, other reactions are possible, such as:

$$4FeO_2H_x + 3CO_2 => Fe_4C_3O_{12} + 2xH_2O + (1-x) \, O_2, \qquad (4)$$

which might have interesting consequences for oxygen fugacity at large depth and by consequence at the Earth's surface.

The P-T conditions at which FeO_2H_x and $Fe_4C_3O_{12}$ have been observed are presented in Fig. 5 along with mantle geotherms and hypothetical slab geotherms [44,45]. The exact chemistry and stability of the high-pressure pyrite-structured FeO_2H_x are still controversial: Nishi *et al.* [35] propose a pyrite-structured oxyhydroxide FeOOH that is stable down to the core–mantle boundary and might undergo dehydration in the D″layer, whereas Hu *et al.* [34] and Liu *et al.* [46] suggest a pyrite-structured peroxide/hydride FeO_2H_x that would undergo progressive dehydrogenation from about 1800-km depth down to the core–mantle boundary. However, our present study demonstrates that the presence of CO_2, produced for example by decarbonation reactions involving silicate phases, could completely alter these interpretations. Indeed, the pyrite-structured FeO_2H_x would react with CO_2 to form a high-pressure carbon-bearing phase $Fe_4C_3O_{12}$ at P-T conditions of the lower-mantle geotherm, as well as of those of a 'hot' slab path (such as Central America slabs [47]), and even on geotherms of cold slabs close to the core–mantle boundary. Unfortunately, we currently lack thermodynamic constraints to evaluate the activity of CO_2 in the mantle and its stability relative to carbonates or C-reduced species. This should be addressed in the future to confirm that $Fe_4C_3O_{12}$-forming reaction actually takes place in the mantle. Although the thermodynamic stability of tetrahedral carbonates with respect to reduced carbon phases is still unknown, it appears that $Fe_4C_3O_{12}$ tetrahedral carbonate is an excellent candidate for a stable carbon host in the lower mantle [15,40]. The carbonation reaction (R3) is associated with release of H_2O. Therefore, the carbonation reaction provides a new mechanism for releasing hydrogen into the deep mantle as H_2O. It adds up to dehydration reactions that take place at shallower depths in subduction settings and to the progressive dehydrogenation of FeOOH at about 1800-km depth [34,46]. Similarly to carbon [12,48], H_2 would be oxidized to produce OH or H_2O through the reduction of Fe^{3+} in silicate minerals during mantle upwelling. Such release of OH or H_2O could trigger partial melting, since H_2O is much more soluble in silicate melts than H_2 [49,50]. In hot subducting slabs, the carbonation reaction from oxyhydroxide may take place as shallow as 1200 km [15], before any transformation of α-FeOOH into FeO_2H_x. In environments rich in iron oxides such as hematite Fe_2O_3 (e.g. in banded iron formation lithology), Fe_2O_3 may directly react
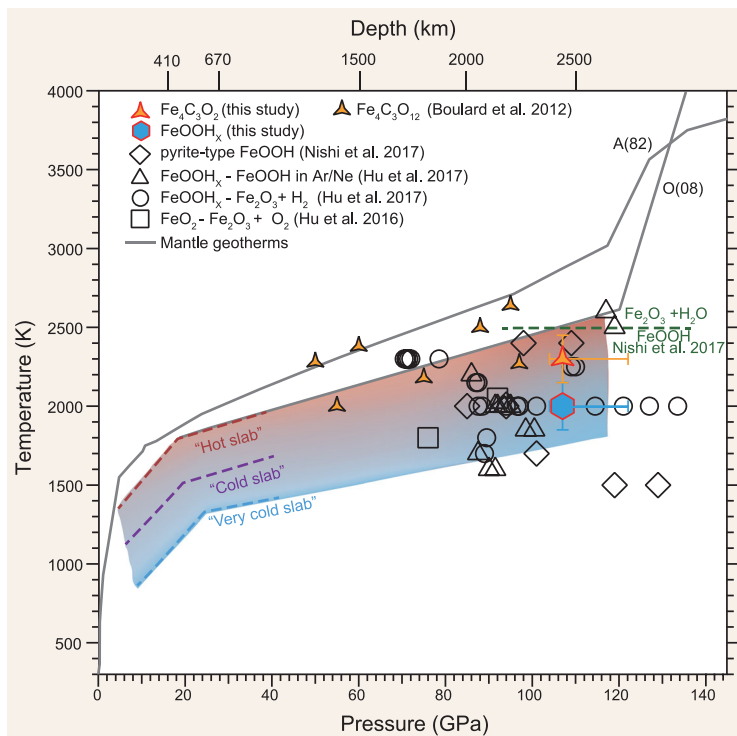
Figure 5. P-T conditions at which the different phases have been observed experimentally: pyrite-structured FeO_2 from Hu *et al.* [37], pyrite-structured FeO_2H_x from this study as well as from Hu *et al.* [34] from both $Fe_2O_3+H_2O$ and FeOOH in Ar/Ne experiments, pyrite-structured FeOOH from Nishi *et al.* [35] and $Fe_4C_3O_{12}$ from the present study as well as from $FeO + CO_2$ experiments in Boulard *et al.* [15]. The mantle geotherms from [59] (O(08)) and [60] (A(82)), as well as hypothetical P-T paths for a 'very cold slab', 'cold slab' and a 'hot slab' [45,61] are also represented for comparison.

with CO_2 [15] without implication of FeOOH in the chemical reaction. In this latter scenario, carbon and hydrogen would be both transported in the deep mantle without dehydrogenation due to carbonation (although it is possible that slow dehydrogenation of FeO_2H_x takes place [34]). The degree of coupling between the deep carbon and hydrogen cycles is therefore strongly dependent on the local mineralogical and chemical environment. Because carbonates are also potential oxidized carbon carriers, additional studies on the interaction between carbonates and FeOOH should be carried out in order to provide a comprehensive model for the deep-mantle carbon and water cycles. Nevertheless, the transformation reported here would prevent the production of FeH_x, which is expected by the reaction of iron alloy from the core and hydrous phase at the core–mantle boundary [28,35,51]. This might have favored transfer of carbon to the core rather than of hydrogen during early Earth differentiation and therefore provide a mechanism for high amounts of C in an O-rich core [52].

MATERIALS AND METHODS

Experiments were conducted using symmetric Mao-Bell-type DAC equipped with 300/100-μm beveled culet diamonds and rhenium gasket with 30-μm starting diameter hole and 25-μm starting thickness. Natural sample of crystalline goethite (α-FeOOH) from lateritic soil in Central African Republic was provided by the collection of University Pierre et Marie Curie. FeOOH was loaded in CO_2 together with a ruby ball (see Supplementary Fig. 1 for an XRD characterization before the experiment). The CO_2 gas was loaded using high-pressure gas-loading apparatus at room temperature and 600 bars. FeOOH was isolated from diamonds by CO_2, preventing reactions with diamonds.

In situ angle-dispersive XRD measurements were performed on the high-pressure beamline ID-27 at the European Synchrotron Radiation Facility (ESRF) using a monochromatic incident X-ray beam of 0.3738-Å wavelength. Before the experiments, the X-ray spot, spectrometer entrance and the heating laser spot were carefully aligned. The sample was first pressurized to its target pressure (107 GPa) before laser heating. Pressure was measured using ruby fluorescence before and after laser heating at room temperature by the use of a blue laser [53]. XRD peaks from the Re-gasket collected across the diamond culet gave pressures between 101 and 107 GPa. Two YAG lasers with excellent power stability were aligned on both sides of the sample, which produce hot spots larger than 20-μm (FWHM) diameter. Temperatures were obtained by fitting the sample thermal emission spectrum from the central $2 \times 2\ \mu m^2$ of the hotspot to the Planck's function using the wavelength range 600–900 nm. Reflective lenses were used for measurement in order to prevent any chromatic aberration [54]. The monochromatic X-ray beam was focused to 3×3 micron. This is smaller than the laser heating spot in order to reduce both the radial and axial temperature gradients. Typical exposure time was 30 s at high pressures and high temperatures. The diffraction images were integrated with the Fit2d software [57]. The 1D diffraction patterns were treated with the General Structure Analysis System (GSAS) software package [58] using the Rietveld or Lebail methods to identify the different phases and refine lattice parameters. During heating and XRD acquisition, temperature was measured continuously. Temperature uncertainties are estimated to be of about 150 K [55]. At high temperatures, thermal pressure corrections are of the order of +10–15% of the initial pressure [56].

Raman spectra were collected at high pressure and ambient temperature after transformation of the

sample. We used a Jobin–Yvon$^{®}$ HR-460 spectrometer with monochromator with 1500 gratings/mm, equipped with an Andor$^{®}$ CCD camera. Raman signal was excited using the 514.5-nm wavelength of an Ar^{+} laser, delivering 300 mW focused into a 2-μm spot by a long-working distance Mitutoyo$^{®}$ x20 objective.

A focused ion beam (FIB) thin section was extracted from the recovered sample at the center of laser-heated spot and thinned to electron transparency ($\sim$100-nm thickness). FIB milling was performed using a FEI STRATA DB 235 at IEMN (Lille, France) with a focused Ga^{+} ion beam operating at 30 kV and currents from 20 nA down to 1 pA for final surfacing. Analytical transmission electron microscopy (ATEM) was carried out on the FIB thin section with a JEOL 2100-F operating at 200 keV, equipped with a field emission gun. Semi-quantitative chemical analyses on the individual phases was obtained by X-ray energy dispersive spectrometry (XEDS) and SAED patterns were used for phase identification.

SUPPLEMENTARY DATA

Supplementary data are available at *NSR* online.

ACKNOWLEDGEMENTS

REFERENCES

1. Kelemen PB and Manning CE. Reevaluating carbon fluxes in subduction zones, what goes down, mostly comes up. *Proc Natl Acad Sci USA* 2015; **112**: E3997–4006.
2. Van Keken PE, Hacker BR and Syracuse EM *et al.* Subduction factory: 4. Depth-dependent flux of H_2O from subducting slabs worldwide. *J Geophys Res* 2011; **116**: B01401.
3. Alt JC and Teagle DAH. The uptake of carbon during alteration of ocean crust. *Geochim Cosmochim Acta* 1999; **63**: 1527–35.
4. Sleep NH and Zahnle K. Carbon dioxide cycling and implications for climate on ancient Earth. *J Geophys Res* 2001; **106**: 1373–99.
5. Macpherson CG, Hilton DR and Hammerschmidt K. No slab-derived CO_2 in Mariana Trough back-arc basalts: implications for carbon subduction and for temporary storage of CO_2 beneath slow spreading ridges. *Geochem Geophys Geosyst* 2010; **11**: 1–25.
6. Javoy M. The major volatile elements of the Earth: their origin, behavior, and fate. *Geophys Res Lett* 1997; **24**: 177–80.
7. Ohtani E. Hydrous minerals and the storage of water in the deep mantle. *Chem Geol* 2015; **418**: 6–15.
8. Keppler H, Wiedenbeck M and Shcheka SS. Carbon solubility in olivine and the mode of carbon storage in the Earth's mantle. *Nature* 2003; **424**: 414–6.
9. Shcheka SS, Wiedenbeck M and Frost DJ *et al.* Carbon solubility in mantle minerals. *Earth Planet Sci Lett* 2006; **245**: 730–42.
10. Dasgupta R and Hirschmann MM. The deep carbon cycle and melting in Earth's interior. *Earth Planet Sci Lett* 2010; **298**: 1–13.
11. Frost DJ and McCammon CA. The redox state of Earth's mantle. *Annu Rev Earth Planet Sci* 2008; **36**: 389–420.
12. Rohrbach A and Schmidt MW. Redox freezing and melting in the Earth's deep mantle resulting from carbon-iron redox coupling. *Nature* 2011; **472**: 209–12.
13. Boulard E, Gloter A and Corgne A *et al.* New host for carbon in the deep Earth. *Proc Natl Acad Sci USA* 2011; **108**: 5184–7.
14. Dasgupta R, Hirschmann MM and Withers AC. Deep global cycling of carbon constrained by the solidus of anhydrous, carbonated eclogite under upper mantle conditions. *Earth Planet Sci Lett* 2004; **227**: 73–85.
15. Boulard E, Menguy N and Auzende A-L *et al.* Experimental investigation of the stability of Fe-rich carbonates in the lower mantle. *J Geophys Res* 2012; **117**: B02208.
16. Boulard E, Pan D and Galli G *et al.* Tetrahedrally coordinated carbonates in Earth's lower mantle. *Nat Commun* 2015; **6**: 6311.
17. Merlini M, Hanfland M and Salamat A *et al.* The crystal structures of $Mg_2Fe_2C_4O_{13}$ with tetrahedrally coordinated carbon, and $Fe_{13}O_{19}$, synthesized at deep mantle conditions. *Ame Mineral* 2015; **100**: 2001–4.
18. Stachel T, Harris W and Brey GP. Kankan diamonds (Guinea) II: lower mantle inclusion parageneses. *Contrib Mineral Petrol* 2000; **140**: 16–27.
19. Brenker FE, Vollmer C and Vincze L *et al.* Carbonates from the lower part of transition zone or even the lower mantle. *Earth Planet Sci Lett* 2007; **260**: 1–9.
20. Takafuji N, Fujino K and Nagai T *et al.* Decarbonation reaction of magnesite in subducting slabs at the lower mantle. *Phys Chem Minerals* 2006; **33**: 651–4.
21. Seto Y, Hamane D and Nagai T *et al.* Fate of carbonates within oceanic plates subducted to the lower mantle, and a possible mechanism of diamond formation. *Phys Chem Minerals* 2008; **35**: 223–9.
22. Litasov KD, Goncharov AF and Hemley RJ. Crossover from melting to dissociation of CO_2 under pressure: implications for the lower mantle. *Earth Planet Sci Lett* 2011; **309**: 318–23.
23. Bolfan-casanova N, Keppler H and Rubie DC. Water partitioning between nominally anhydrous minerals in the MgO-SiO_2-H_2O system up to 24 GPa: implications for the distribution of water in the Earth's mantle. *Earth Planet Sci Lett* 2000; **182**: 209–21.
24. Jacobsen SD, Demouchy S and Frost DJ *et al.* A systematic study of OH in hydrous wadsleyite from polarized FTIR spectroscopy and single-crystal X-ray diffraction: oxygen sites for hydrogen storage in Earth's interior. *Am Mineral* 2005; **90**: 61–70.

25. Pearson DG, Brenker FE and Nestola F *et al.* Hydrous mantle transition zone indicated by ringwoodite included within diamond. *Nature* 2014; **507**: 221–4.

26. Ohtani E. Water in the mantle. *Elements* 2005; **1**: 25–30.

27. Nishi M, Irifune T and Tsuchiya J *et al.* Stability of hydrous silicate at high pressures and water transport to the deep lower mantle. *Nat Geosci* 2014; **7**: 2–5.

28. Ohira I, Ohtani E and Sakai T *et al.* Stability of a hydrous δ-phase, AlOOH-MgSiO$_2$(OH)$_2$, and a mechanism for water transport into the base of lower mantle. *Earth Planet Sci Lett* 2014; **401**: 12–7.

29. Pamato MG, Myhill R and Bo T *et al.* Lower-mantle water reservoir implied by the extreme stability of a hydrous aluminosilicate. *Nature Geosci* 2015; **8**: 75–9.

30. Tsuchiya J. First principles prediction of a new high-pressure phase of dense hydrous magnesium silicates in the lower mantle. *Geophys Res Lett* 2013; **40**: 4570–3.

31. Suzuki A, Ohtani E and Kamada T. A new hydrous phase d-AlOOH synthesized at 21 GPa and 1000°C. *Phys Chem Miner* 2000; **27**: 689–93.

32. Tsuchiya J, Tsuchiya T and Tsuneyuki S *et al.* First principles calculation of a high-pressure hydrous phase, δ-AlOOH. *Geophys Res Lett* 2002; **29**: 15-1–15-4.

33. Gleason AE, Jeanloz R and Kunz M. Pressure-temperature stability studies of FeOOH using X-ray diffraction. *Am Mineral* 2008; **93**: 1882–5.

34. Hu Q, Kim DY and Liu J *et al.* Dehydrogenation of goethite in Earth's deep lower mantle. *Proc Natl Acad Sci USA* 2017; **114**: 1498–501.

35. Nishi M, Kuwayama Y and Tsuchiya J *et al.* The pyrite-type high-pressure form of FeOOH. *Nature* 2017; **547**: 205–8.

36. Mao H, Hu Q and Yang L *et al.* When water meets iron at Earth's core-mantle boundary. *Natl Sci Rev* 2017; **4**: 870–8.

37. Hu Q, Kim DY and Yang W *et al.* FeO$_2$ and FeOOH under deep lower-mantle conditions and Earth's oxygen–hydrogen cycles. *Nature* 2016; **534**: 241–4.

38. Tsuchiya J and Tsuchiya T. First-principles prediction of a high-pressure hydrous phase of AlOOH. *Phys Rev B—Condens Matter Mater Phys* 2011; **83**: 2–5.

39. Liu J, Lin J-F and Prakapenka VB. High-pressure orthorhombic ferromagnesite as a potential deep-mantle carbon carrier. *Sci Rep* 2015; **5**: 7640.

40. Cerantola V, Bykova E and Kupenko I *et al.* Stability of iron-bearing carbonates in the deep Earth's interior. *Nat Comms* 2017; **8**: 15960.

41. Iota V, Yoo C-S and Klepeis J-H *et al.* Six-fold coordinated carbon dioxide VI. *Nature Mater* 2007; **6**: 34–8.

42. Goncharov AF, Struzhkin V and Mao H *et al.* Raman spectroscopy of dense H$_2$O and the transition to symmetric hydrogen bonds. *Phys Rev Lett* 1999; **83**: 1998–2001.

43. Bove LE, Gaal R and Raza Z *et al.* Effect of salt on the H-bond symmetrization in ice. *Proc Natl Acad Sci USA* 2015; **112**: 8216–20.

44. Ohtani E and Maeda M. Density of basaltic melt at high pressure and stability of the melt at the base of the lower mantle. *Earth Planet Sci Lett* 2001; **193**: 69–75.

45. Komabayashi T. Petrogenetic grid in the system MgO-SiO$_2$-H$_2$O up to 30 GPa, 1600°C: applications to hydrous peridotite subducting into the Earth's deep interior. *J Geophys Res* 2004; **109**: B03206.

46. Liu J, Hu Q and Young Kim D *et al.* Hydrogen-bearing iron peroxide and the origin of ultralow-velocity zones. *Nature* 2017; **551**: 494–7.

47. Syracuse EM, Keken PE Van and Abers GA *et al.* The global range of subduction zone thermal models. *Phys Earth Planet Inter* 2010; **183**: 73–90.

48. Stagno V, Ojwang DO and McCammon CA *et al.* The oxidation state of the mantle and the extraction of carbon from Earth's interior. *Nature* 2013; **493**: 84–8.

49. Yang X, Keppler H and Li Y. Molecular hydrogen in mantle minerals. *Geochem Persp Let* 2016; **2**: 160–8.

50. Hirschmann MM, Withers AC and Ardia P *et al.* Solubility of molecular hydrogen in silicate melts and consequences for volatile evolution of terrestrial planets. *Earth Planet Sci Lett* 2012; **345–348**: 38–48.

51. Terasaki H, Ohtani E and Sakai T *et al.* Stability of Fe-Ni hydride after the reaction between Fe-Ni alloy and hydrous phase (δ-AlOOH) up to 1.2Mbar: possibility of H contribution to the core density deficit. *Phys Earth Planet Inter* 2012; **194–195**: 18–24.

52. Morard G, Andrault D and Antonangeli D *et al.* Fe–FeO and Fe–Fe$_3$C melting relations at Earth's core–mantle boundary conditions: implications for a volatile-rich or oxygen-rich core. *Earth Planet Sci Lett* 2017; **473**: 94–103.

53. Mao HK, Xu J and Bell PM. Calibration of the Ruby Pressure Gauge to 800 kbar under quasi-hydrostatic conditions. *J Geophys Res* 1986; **91**: 4673–6.

54. Benedetti LR and Loubeyre P. Temperature gradients, wavelength-dependent emissivity, and accuracy of high and very-high temperatures measured in the laser-heated diamond cell. *High Press Res* 2004; **24**: 423–45.

55. Morard G, Andrault D and Guignot N *et al.* In situ determination of Fe–Fe$_3$S phase diagram and liquid structural properties up to 65 GPa. *Earth Planet Sci Lett* 2008; **272**: 620–6.

56. Fiquet G, Auzende AL and Siebert J *et al.* Melting of peridotite to 140 gigapascals. *Science* 2010; **329**: 1516–8.

57. Hammersley AP, Svensson SO and Hanfland M *et al.* Two-dimensional detector software: from real detector to idealised image or two-theta scan. *High Pressure Res* 1996; **14**: 235–48.

58. Larson AC and Von Dreele RB. General Structure Analysis System (GSAS). *Los Alamos Natl Lab Rep LAUR* 2004, 86–748.

59. Ono S. Experimental constraints on the temperature profile in the lower mantle. *Phys Earth Planet Inter* 2008; **170**: 267–73.

60. Anderson OL. The Earth's core and the phase diagram of iron. *Philos Trans R Soc A Math Phys Eng Sci* 1982; **306**: 21–35.

61. Maeda F, Ohtani E and Kamada S *et al.* Diamond formation in the deep lower mantle: a high-pressure reaction of MgCO$_3$ and SiO$_2$. *Sci Rep* 2017; **7**: 40602.